Hindawi Publishing Corporation
Smart Materials Research
Volume 2013, Article ID 498019, 16 pages
http://dx.doi.org/10.1155/2013/498019

Research Article

Development and Application of One-Sided Piezoelectric Actuating Micropump

H. K. Ma, Y. T. Li, H. C. Su, W. F. Luo, T. J. Pan, F. M. Fang, and S. W. Hsu

Department of Mechanical Engineering, National Taiwan University, No. 1, Sec. 4, Roosevelt Road, Taipei 10617, Taiwan

Correspondence should be addressed to H. K. Ma; skma@ntu.edu.tw

Received 8 March 2013; Accepted 4 September 2013

Academic Editor: Osama J. Aldraihem

Three types of one-sided actuating piezoelectric micropumps are studied in this paper. In the first type, one-sided actuating micropump with two check valves can enhance the flow rate and prevent the back flow in suction mode to keep the flow in one direction. Furthermore, the frequency modulator is applied in the micropump to adjust and promote the maximum flow rate higher than 5.0 mL/s. In the second type, valveless micropump with secondary chamber shows that the secondary chamber plays a key role in the application of the valveless micropump. It not only keeps the flow in one direction but also makes the flow rate of the pump reach 0.989 mL/s. In addition, when a nozzle/diffuser element is used in valveless micropump, the flow rate can be further improved to 1.183 mL/s at a frequency of 150 Hz. In the third type, piezoelectric actuating pump is regarded as an air pump in the application of a microfuel cell system, which can increase more air inlet to improve the fuel/air reaction and further increase the performance of fuel cell.

1. Introduction

In recent years, micropump plays a significant role in many fields, specifically in chemical, medical, and thermal managements. Since there are distinct requirements in each field, several types of micropumps have been designed to meet those requirements. Micropumps, which have the advantage of small size and configurable dimension, are gradually becoming one of the solutions for electronic heat dissipation. There are several types of actuation approaches in developing, such as electromagnetic [1, 2], piezoelectric [3, 4], shape memory alloy [5], electrostatic [6], and thermopneumatic [7] devices. Most of actuations are complicated in structure and have great energy consumption. However, piezoelectric actuation has the notable advantages that are a relatively simple component and energy consumption.

Micropumps can be categorized into two major types: displacement pumps [8–10] and dynamic pumps [11, 12]. Displacement pumps use the moving mechanical part to change the volume of the chamber, such as the one-sided actuating diaphragm pumps. Dynamic pumps usually utilize the interactions of the fluid with an electric or magnetic field, which continuously applies force on working fluid. Electrohydrodynamic [11] and magnetohydrodynamic [12] are the examples of dynamic pump. Considering flow direction elements, micropumps can be classified as with or without valves. The first prototype of a valveless pump consisting of a circular cylindrical volume where the top had a thin brass diaphragm to which a piezoelectric disc was fixed and its flow rate was 0.26 mL/s [3].

Ma et al. [13, 14] developed a one-sided actuating piezoelectric micropump with two check valves to drive liquid for the application on cooling system. Later the improved design demonstrated a maximum flow rate of 2.35 mL/s and a maximum pump head of 6.4 kPa. In 2008, the further design showed that the maximum flow rate was 4.4 mL/s and the maximum pump head was 8.33 kPa under ±50 V [15]. Moreover, in 2011, valveless micropump with two chambers has been developed to actuate fluid at a higher flow rate in one direction by adding a secondary chamber. The flow rate of pump can reach 0.989 mL/s, and the maximum pump head is 1.52 kPa when using the 0.3 mm-thick secondary diaphragm and the 0.5 mm-thick primary diaphragm. In addition, if a nozzle/diffuser element is applied with a secondary chamber,

the flow rate can be improved to 1.183 mL/s at 150 Hz [16]. In this study, the actuation mechanism and performance of one-sided piezoelectric actuating micropump with valve/valveless are discussed. Moreover, the effect of frequency modulator on piezoelectric actuator vibrating amplitude is studied to control the flow rate. The piezoelectric pump is also regarded as an air pump in the application of a microfuel cell system, which can pump more inlet air to increase the fuel/air reaction and further increase the performance of fuel cell.

2. One-Sided Actuating Micropump with Check Valve

A traditional piezoelectric micropump driven by central-actuating, which is shown in Figure 1(a), is a thin, compact, and lightweight microdiaphragm pump. However, it is limited to height, control volume, and mass flow rate due to its actuating displacement in z-direction by piezoelectric effect. It cannot provide greater amplitude and sufficient flow rate. To improve and enhance pump performance, one-sided actuating micropump with two passive checks is developed, shown in Figure 1(b), which is composed of several components, including a case with a chamber, a rectangular piezoelectric material, membrane, and two (inlet/outlet) passive check valves. The piezoelectric material is selected as an actuator. A diaphragm keeps the PZT device from water vapor and helps the actuator to provide more volumetric change in suction and pumping mode. Inlet and outlet valves are placed in one of the chambers to prevent back flow as oscillation liquid passes through the pump chamber. Mechanism of actuating micropump is shown in Figure 2. When the actuator moves downward, the outflow will be in one direction with the inlet valve closed and the outlet valve opened. On the other hand, the actuator moves upward to increase the chamber volume; the inflow will be in the chamber with the inlet valve open and the outlet valve closed. The specification of each design is listed in Table 1 and the geometry of valve is shown in Figure 3(a). Furthermore, after experimental No. 10 the volume of a cooling system is reduced by combining the cold plate with pump chamber, which is shown in Figure 3(b), and studied on the effect of fin in chamber.

2.1. Theoretical Analysis

2.1.1. Pump Chamber Analysis. The liquid is actuated by the piezoelectric device in the pump chamber. The governing equation of the actuating part on the pump chamber can be expressed as

$$F_{\text{input}} \sin\left(2\pi f t\right) - F_d = m\ddot{z} + kz. \tag{1}$$

In the left-hand term, F_{input} represents a force that converts from the input voltage due to the piezoelectric effect, and f is a frequency of the input AC sine waves. F_d is the damping force due to the friction and pump shape (including sudden contraction, expansion, and the valve influence in the chamber); m stands for the total equivalent masses of the piezoelectric device, PDMS diaphragm, and adding liquid [17]; k is the equivalent spring constant of the piezoelectric device and PDMS diaphragm in parallel, as shown in Figure 4(a).

The diaphragm fixed on the chamber is bent by piezoelectric device. Therefore, it can be seen as a fix-end beam and supports a uniform load of intensity q acting over part of the span. The maximum deflection of the diaphragm can be obtained [18]:

$$\delta_{\text{diaph,max}} = \frac{qL_{\text{pzt}}}{24LE_{\text{PDMS}}I_{\text{diaph}}}\left(3L_{\text{pzt}}^4 - 7L_{\text{pzt}}^3L + 4L_{\text{pzt}}^2L^2\right), \tag{2}$$

where E_{PDMS} is Young's modulus of PDMS; L is the length of the pump chamber. It is determined by the uncovered length and the actuator length:

$$L = L_{\text{pzt}} + L_{\text{uc}}. \tag{3}$$

Therefore, the spring constant of the diaphragm is given by

$$k_{\text{diaph}} = \frac{qL_{\text{pzt}}}{\delta_{\text{diaph, max}}} = \frac{24LE_{\text{PDMS}}I_{\text{diaph}}}{3L_{\text{pzt}}^4 - 7L_{\text{pzt}}^3L + 4L_{\text{pzt}}^2L^2}. \tag{4}$$

2.1.2. Valve Analysis. The passive check valve, which is made of PDMS, is an important device in the design of the one-sided actuating diaphragm micropump. The passive check valve decides the performance of the pump. PDMS is an elastic structural element that can be expressed as a spring motion to store and release energy. The governing equation of oscillating motion for valves, which is shown in Figure 4(b), can be expressed by

$$F_{\text{drag}} = m_{\text{va}}\ddot{x} + k_{\text{va}}x, \tag{5}$$

where m_{va} and k_{va} are mass and spring constant of the valve. The left-hand term, F_{drag}, represents the drag force of the valve influenced by the valve's shape and an upstream velocity. It is written as

$$F_{\text{drag}} = \frac{1}{2}C_d\rho A_p u^2, \tag{6}$$

where C_d is the drag coefficient of the valve in the fluid, A_p represents the project area of the valve, and u is the relative velocity of the upstream velocity with respect to the valve velocity, as

$$u = v_{\max}\sin\left(2\pi f t\right) - \dot{x}, \tag{7}$$

where $\dot{x}$ is the valve velocity and $v_{\max}\sin(2\pi f t)$ stands for the upstream velocity generated by the actuator at the frequency f. Assuming that the valve velocity is small compared to the upstream velocity, (6) can be written as

$$F_{\text{drag}} = \frac{1}{2}C_d\rho A_p\left(v_{\max}\sin\left(2\pi f t\right)\right)^2 - C_d\rho A_p v_{\max}\sin\left(2\pi f t\right)\dot{x}. \tag{8}$$

Table 1: Specification of each design.

Experiment case no.	Design of valve			Design of pump chamber		Design of fins		
	Thickness (mm)	Length (mm)	Shape	Chamber size (mm^3)	Inlet/outlet diameter (mm)	Thickness (mm)	Height (mm)	Number of fin
1	0.5	5	O	5 ∗ 45 ∗ 28	2 mm	—	—	—
2	1	5	O	5 ∗ 45 ∗ 28	2 mm	—	—	—
3	1.5	5	O	5 ∗ 45 ∗ 28	2 mm	—	—	—
4	0.5	5	N	5 ∗ 45 ∗ 28	2 mm	—	—	—
5	0.5	5	NC	5 ∗ 45 ∗ 28	2 mm	—	—	—
6	0.5	5	NC	4 ∗ 45 ∗ 28	2 mm	—	—	—
7	0.5	5	OC	5 ∗ 45 ∗ 28	2 mm	—	—	—
8	0.2	5	OC	5 ∗ 45 ∗ 28	2 mm	—	—	—
9	0.2	5	NCW	4 ∗ 45 ∗ 28	2 mm	—	—	—
10	0.2	5	NCW	4 ∗ 45 ∗ 28	2 mm	1	1.25	6
11	0.2	5	NCW	4 ∗ 45 ∗ 28	2 mm	1	2.5	6
12	0.2	5	NCW	4 ∗ 45 ∗ 28	2 mm	0.5	1.25	12
13	0.2	3	NCW	4 ∗ 45 ∗ 28	2 mm	—	—	—
14	0.2	3.5	NCW	4 ∗ 45 ∗ 28	2 mm	—	—	—

O: original valve; N: narrow valve; C: valve with cone; W: with combined design of cold plate and pump chamber.

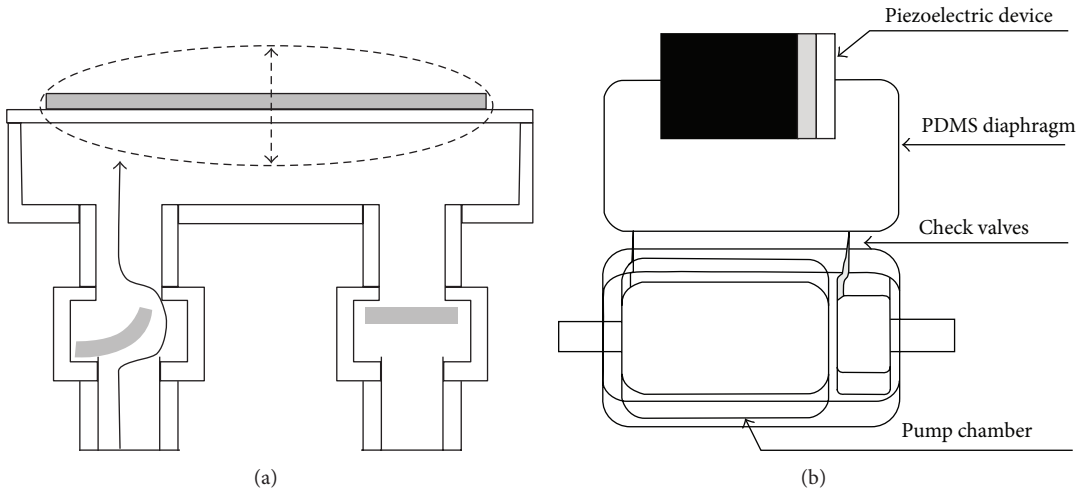

Figure 1: Comparison of the actuating mechanism: (a) traditional micropump and (b) one-sided actuating diaphragm micropump.

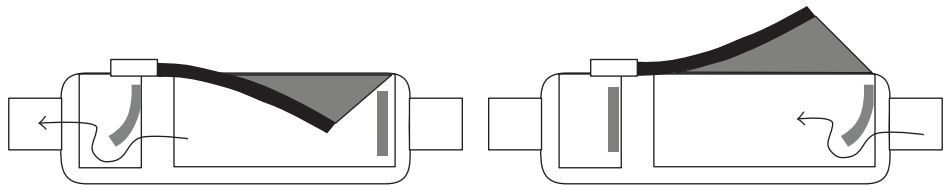

(a) (b)

Figure 2: Mechanism of actuating micropump: (a) outlet and (b) inlet.

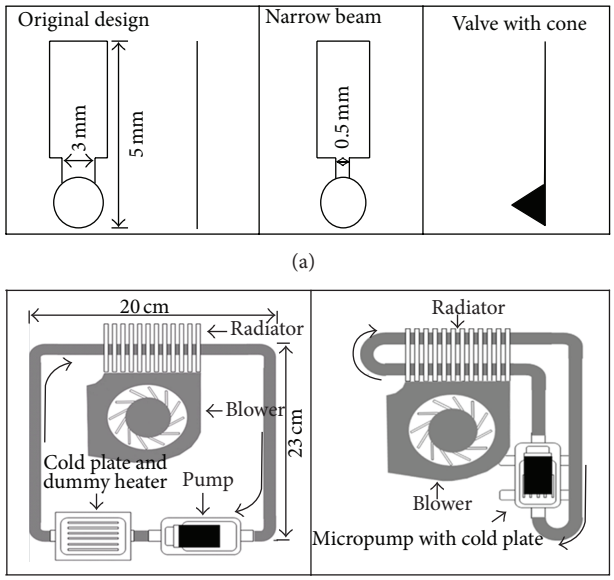

Figure 3: The different geometry type of valve.

Substituting (8) into (5), then

$$\frac{1}{2}C_d\rho A_p(v_{\max}\sin(2\pi ft))^2 = m_{va}\ddot{x} + C_d\rho A_p v_{\max}\sin(2\pi ft)\,\dot{x} + k_{va}x, \quad (9)$$

where the left-hand side of the equation is an external force, and the second term in the right-hand side can be seen as a damping force.

In this study, the shape of the check valve can be considered as a cantilever beam. The bending moment is a function of position along the valve, and the deformation of the valve is small. If there is a concentrated load at the valve's free end as shown in Figure 4, then the spring constant K_{va} of the cantilever valve can be expressed as

$$K_{va} = \frac{3E_{PDMS}I_{va}}{L_{va}^3}, \quad (10)$$

where $I_{va} = bh^3/12$ is the second moment of area of a rectangular section and L_{va} is the length of the valve.

2.2. The Performance of Micropump with Different Diaphragm Uncovered Length. The curvature change of actuating diaphragm which determines the behavior of oscillating flow is a great effect on the flow rate. Flow rate is proportional to the volumetric change of pump chamber. To obtain the maximum volumetric change and deflection of the pump diaphragm, the uncovered length of actuator diaphragm should be decided. The effect of uncovered length on flow rate is measured, which is shown in Figure 5. From Figure 5, it is observed that the maximum flow rate changes as the uncovered length increases until it reaches the optimal value (L_{uc} = 6 mm). The diaphragm of uncovered length not only affects the spring constant but also decides the vibrating modes of the actuator. The vibrating modes are defined as "central" at $L_{uc} = 0$ and as "one sided" at $L_{uc} > 0$. Theoretically, the spring constant influences the natural frequency, deflection, and the vibrating mode which involves the liquid motion in the chamber. In the central mode (L_{uc} = 0 mm), there is only 4 mL liquid per minute. Therefore, the central vibration is not applicable as the inlet and outlet are on the side.

2.3. Parametric Studies in Chamber

2.3.1. Effect of Chamber Depth. Compared to No. 5 and No. 6, which is 5 mm and 4 mm in depth separately, Figure 6 shows the performance of pump with different depth. The working fluid inside is oscillated with a piezoelectric device, which is governed by mass, spring, and damping vibration system. Therefore, different type of pump can cause different result even if all conditions are the same except depth. The smaller the depth of chamber is, the smaller the fluid inside chamber will be. Consequently, the less drag force in 4 mm depth can improve the flow rate of pump.

2.3.2. Effect of Fin in Chamber. In general, heat dissipation performance is determined by the flow rates and surface area of the fins. According to (1), the fluid damping effect caused by flow resistance is directly determined by the fin design in the pump chamber. Increasing the height of fins may decrease the flow rate due to the larger flow resistance. The performance of the pumps with six fins that have different heights is shown in Figure 7. Compared with the pump without fins, the flow rate of No. 11, the pump with 2.5 mm-high fins, will drop from 2.1 mL/s to 1.68 mL/s. However, it has a negligible effect on the flow rate when the fins are less than 1.25 mm high. Adding fins in a pump chamber can also increase the area of fins. With the same height of fins, the number of fins in No. 10 is 6 while it is 12 in No. 12. The comparison on flow rates is illustrated

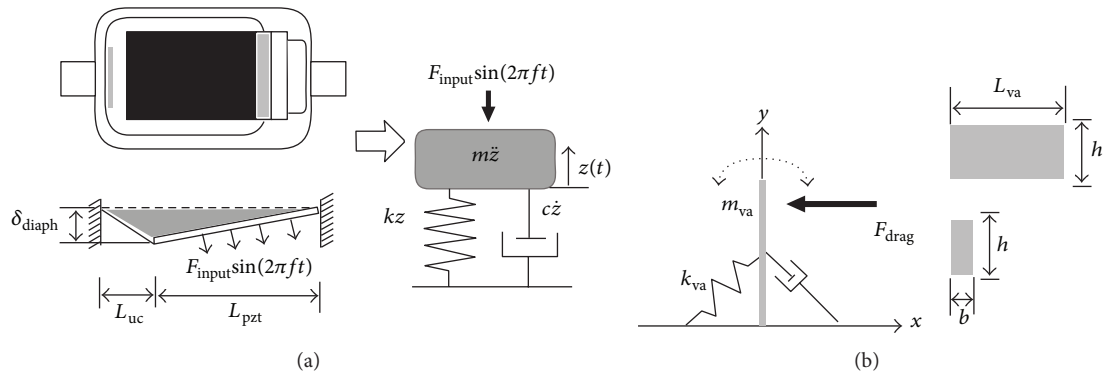

Figure 4: Free body diagram: (a) one-sided motion and (b) valve motion.

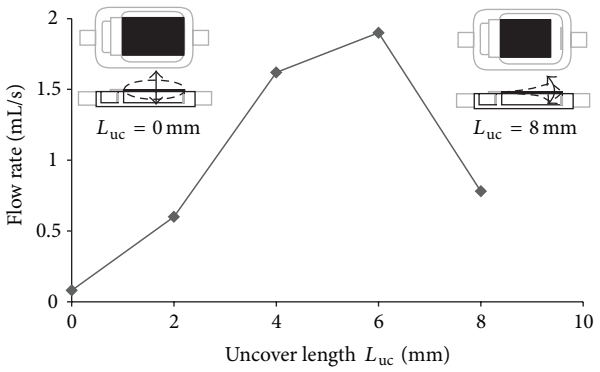

Figure 5: The effect of uncovered length on flow rate (chamber size: $5 * 45 * 28\,mm^3$; valve thickness: 0.5 mm).

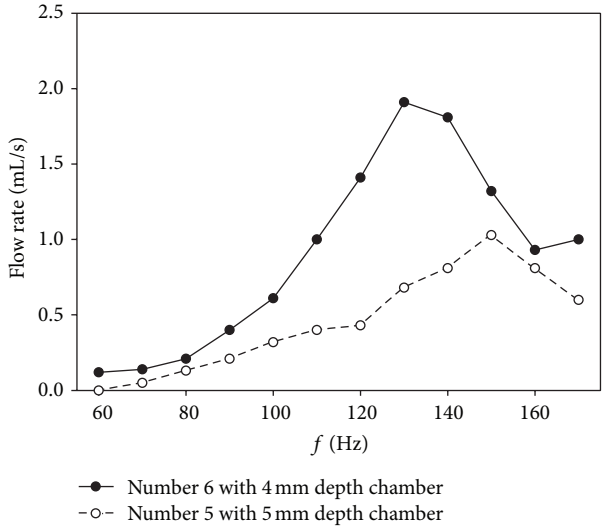

Figure 6: Effect of the chamber depth with different frequency.

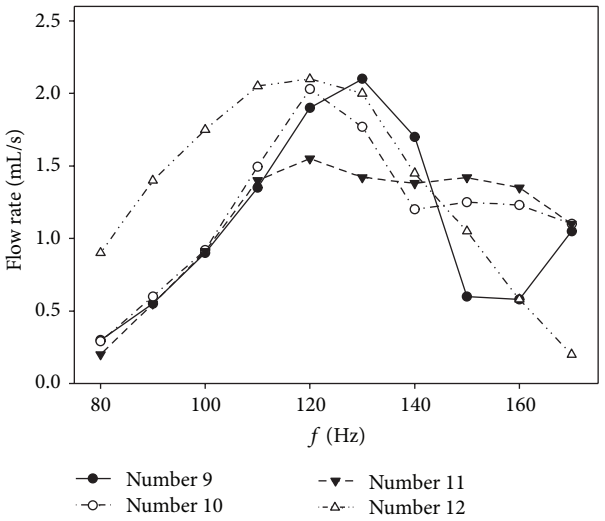

Figure 7: Effect of fin height and number of fin in chamber.

in Figure 7. The maximum flow rate of No. 12 is 2.13 mL/s at 120 Hz, which is close to the maximum flow rate of No. 9.

2.4. The Characteristic of Valve. Because the valves are influenced by the drag force, the pump performance will be better if the motion of the actuator and valves match well. Under a fixed inertia force, the thicker check valve will cause the smaller response acceleration because of the larger spring constant and mass. Therefore, a large delay of valve motion will occur and reduce the oscillating flow rate. On the effect of valve's width, narrow valves are able to respond quickly due to the relatively low damping force. The comparison of valve's width and thickness are shown in Figure 8.

The thickness of the valve will cause different mass and spring constant, as shown in (5). The effect of valve thickness can be found by No. 1, No. 2 with No. 3, and No. 7 with No.8. The maximum flow is 0.58 mL/s in No. 1 while the maximum flow rate in No. 2 and No. 3 are 0.3 mL/s and 0.11 mL/s separately. The drag force is a function of drag coefficient and valve's project area shown in (6). The drag coefficient is affected by the shape of the valves. Therefore, the pump performance changes if the valve's width is reduced. Narrow valves are able to respond quickly due to the relatively low damping force. Comparing No. 1, No. 4, No. 5, and No. 7 with the valve's shape is also shown in Figure 8. The maximum flow

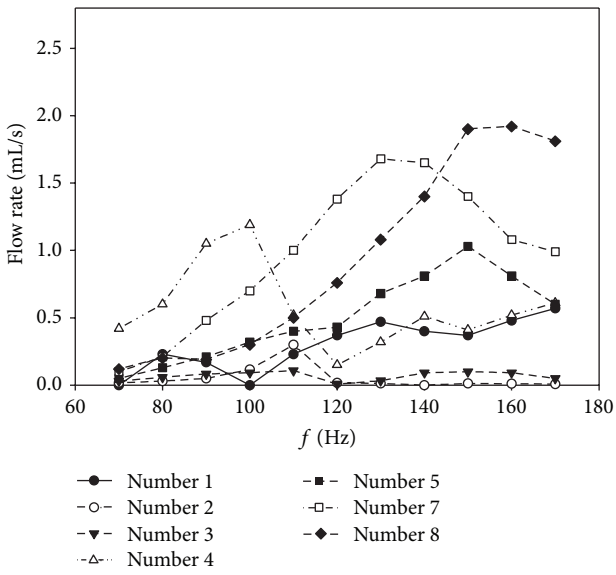

Figure 8: The comparison of flow rates in different valve design.

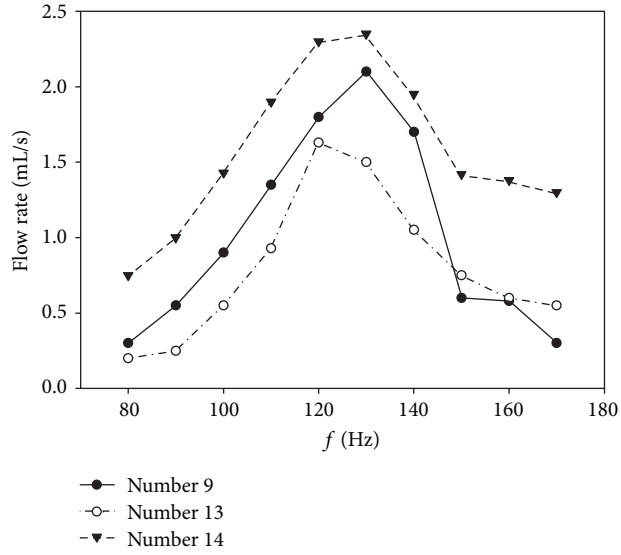

Figure 9: Measured flow rates of the pump with different valve lengths (without fin).

is 1.68 mL/s found in No. 7. A thin narrow valve may vibrate irregularly in non-uniform flow resulting in less flow rate.

The length valve can influence the valve spring constant. For example, the spring constant is larger when the valve's length is shorter. The larger spring constant makes the valves respond faster. The difference of valve length is shown in Figure 9. The pump performs better with a 3.5 mm outlet valve (No. 14) than with a 5 mm valve (No. 9). Nevertheless, when the spring constant is too large, it reduces the vibration of the valve. The local maximum flow rate with the 3.5 mm outlet valve was 2.35 mL/s at 130 Hz, while the local maximum flow rate with the 3 mm outlet valve was only 1.63 mL/s at 120 Hz.

2.5. One-Sided Actuating Diaphragm Micropump with Frequency Modulator. For studying the performance of micropump with frequency modulator, the schematic of experimental micropump is shown in Figure 10(a). It is noteworthy that the experimental instrument just includes one passive check valve to prevent backflow in pumping mode. The rectangular piezoelectric device selected as an actuator is fixed by a frequency modulator.

The resonant frequency of a vibrating plate with one fixed-end is related to density, Poisson's ratio, Young's modulus, length and thickness of the vibrating plate respectively [19]. In addition, the fixed end of PZT plate also can influence the piezoelectric material resonant frequency [20]. Therefore, a frequency modulator is developed to find the maximum amplitude of the PZT plate and increase the displacement of diaphragm to improve the pump flow rate. Figure 10(b) shows the design of a frequency modulator. The main component are two screws (diameter = 3 mm) which can be used to fasten the PZT plate. The screws can be tightened or loosened to modulate the force, F and F_c. F_c is invariable force in the whole experiments. Therefore, F is the only parameter which can affect the boundary condition. F can be adjusted by turning the screw in a frequency modulator.

The characteristics of a frequency modulator can be found by the relation between the resonant frequency and variable force, F. Figure 11 shows a way to investigate the influence of F. At first, the screw is turned in a clockwise direction until it touches the PZT plate where the position of the screw is defined as 0°. Then, the frequency is adjusted gradually until the maximum amplitude appears. During the experiment, the voltage set up as ±60 V, the amplitude and the frequency are recorded every 45° turning.

Figure 12 shows that the resonant frequency is 47.5 Hz when the position of the screw is 0°. When the position of screw is 315°, the resonant frequency is increased to 66.5 Hz. It implies that the exerted higher variable force, F, the resonant frequency will be increased.

Figure 13 shows the amplitude of the PZT plate with frequency modulator. The working condition is under ±100 V and 15–80 Hz. The amplitude of the PZT plate can be enlarged in the range of 35–75 Hz and the maximum amplitude can be found to be 13 mm at 55 Hz by adjusting a frequency modulator. When the micropump is coupling with the adjustable frequency modulator, the maximum flow rate can be adjusted from 14.6 mL/min to 26 mL/min at 45 Hz and ±100 V, shown in Figure 14.

2.6. Summary of One-Sided Actuating Diaphragm Micropump with Check Valve. Comparing with central actuating valveless pump [3], a diaphragm pump with two check valves can direct the flow rate. Moreover, it also can overcome higher flow resistance and improve the performance. However, the resonant frequencies of pump and valve may lose their harmonic motion and drop the actuating force in a lasting operation period. Also, pump may lose its harmonic motion

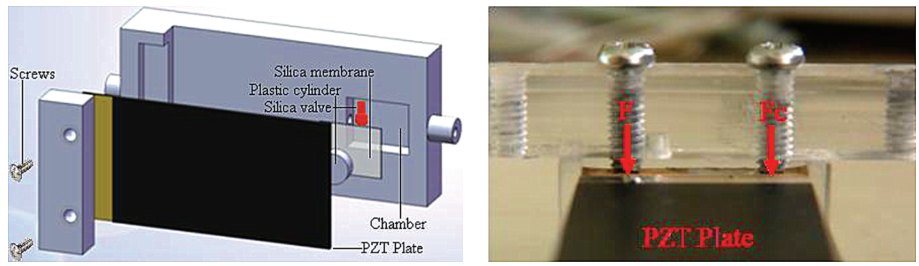

(a) (b)

FIGURE 10: (a) Schematic view of the micropump and a frequency modulator. (b) The design of a frequency modulator.

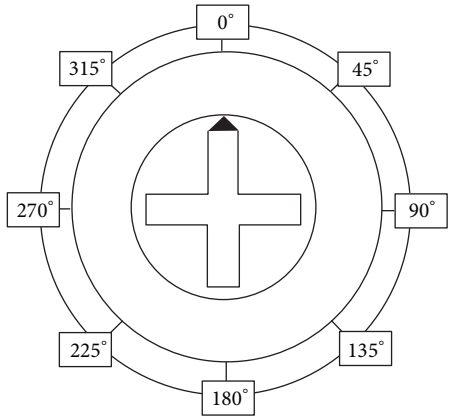

FIGURE 11: Position of the screw.

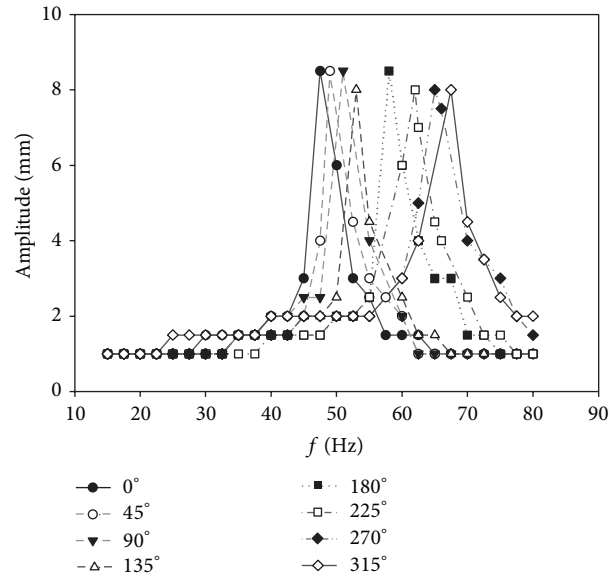

FIGURE 12: Influence of the applied force (F) on the resonant frequency.

due to the fatigue of the PDMS valves because of high-frequency and voltage operations. Furthermore, if the one-sided micropump with check valve works in a high-frequency case, the valve may lose its effectiveness on controlling flow direction and drop the reliability of micropump.

3. One-Sided Actuating Valveless Micropump with a Secondary Chamber

In order to improve the reliability of micropump, Ma et al. [16] developed the mechanism and experimental study of valveless micropump with secondary chamber. The results of valveless pump are discussed below.

3.1. The Mechanism of Valveless Micropump with a Secondary Chamber. The secondary chamber is located between the primary chamber and the outlet. The design of chamber and the operation mechanism of valveless pump are shown in Figures 15(a) and 15(b). In suction mode, the net flow rate is toward the primary chamber. However, the quantity of the net flow rate from the outlet is less than that from the inlet because of the higher flow resistance in the secondary chamber. Therefore, during suction mode, the secondary diaphragm can effectively obstruct the stream and reduce the backflow toward the primary chamber. On the other hand, the secondary diaphragm moves upward to drain fluid out

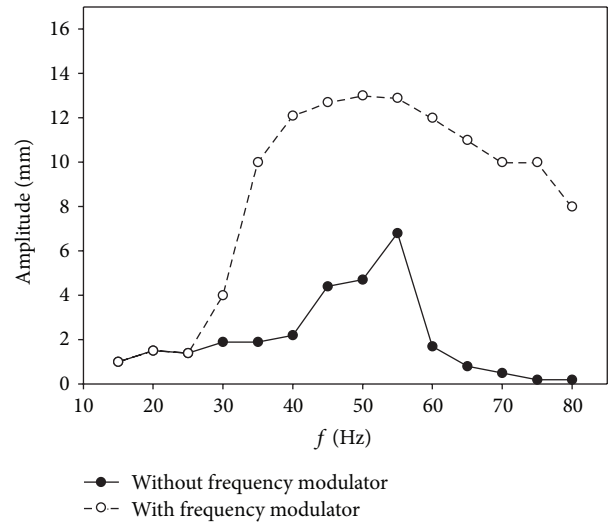

FIGURE 13: Influence of a frequency modulator on the amplitude of the PZT plate.

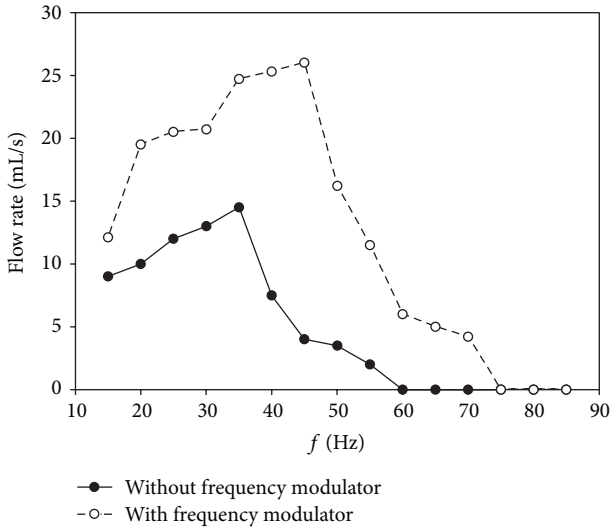

Figure 14: Influence of a frequency modulator on the pump flow rate.

and has a lower flow resistance during pumping mode. The secondary chamber can facilitate the net flow rate toward the outlet throughout a full cycle.

Theoretical analyses of valveless are also applied in (1). It is rewritten in

$$F_{\text{input}} \sin(2\pi f t) = m\ddot{z} + C\dot{z} + kz. \tag{11}$$

Comparing with (1), $C\dot{z}$ represents damping force F_d, and C is the total equivalent damping coefficient due both to inertia effects and to viscous losses of the fluid in the primary chamber. Because the diaphragm fixed on the chamber is bent by the piezoelectric device, the total equivalent spring constant, k, can be written as

$$k = k_{\text{diaph}} + k_{\text{pzt}} = \frac{24\alpha L E_{\text{PDMS}} I_{\text{diaph}}}{3L_{\text{pzt}}^4 - 7L_{\text{pzt}}^3 L + 4L_{\text{pzt}}^2 L^2} + k_{\text{pzt}}, \tag{12}$$

where α is considered a coefficient of the spring constant due to the four fixed edges of the diaphragm on the primary chamber.

In terms of the actuator, the amplitude of the diaphragm, Z, is mainly affected by the spring constant, the damping coefficient, and the frequency. Therefore, (13) is employed to explain the vertical displacement of the diaphragm:

$$\frac{Zk}{F_{\text{input}}} = \frac{1}{\sqrt{\left[1 - (\omega/\omega_n)^2\right]^2 + \left[2\zeta(\omega/\omega_n)\right]^2}}, \tag{13}$$

where ζ is the damping factor, which is defined as

$$\zeta = \frac{C}{2m\omega_n}. \tag{14}$$

The vertical displacement, Z, satisfies the following function [21–23]:

$$\frac{Eh^3}{12(1-\nu^2)}\nabla^4 Z + h\rho_m \frac{\partial^2 Z}{\partial t^2} = F_{\text{input}}(2\pi f t) - P. \tag{15}$$

P is the dynamic pressure exerted on the primary diaphragm by the fluid, which can be calculated using (15) because F_{input} is assumed to be a constant and because Z can be inferred from (13). It is supposed that the pressure of the primary chamber is uniform. Thus, the time-dependent volumetric displacement ΔV can be calculated using (16) [24]:

$$\Delta V = V_0 [1 - \cos(\omega t)] - V_0 \left(\frac{P_0 - P_{\text{atm}}}{P_b - P_{\text{atm}}}\right), \tag{16}$$

where V_0 is the maximum volumetric amplitude caused by a vibrating piezoelectric plate. The second term is the volumetric amplitude caused by the pressure difference between the chamber and the atmosphere, where P_b is defined as the blocking pressure that causes the diaphragm to move a maximum volumetric amplitude.

After differentiating (16) over the time field, the volumetric displacement rate, dV/dt, can be expressed as a net flow rate due to mass conservation, and the effect of the pressure difference on the volumetric amplitude can be neglected with the assumption of a large P_b. Therefore, the equation can be simplified to

$$Q_{\text{out}} - Q_{\text{in}} = V_0 \omega \sin(\omega t). \tag{17}$$

In order to calculate Q_{out}, Q_{in} is substituted by a function of Q_{out}, ξ_i, $\xi_{p,t}$,$\xi_{c,t}$, and P. Thus, the roots of the equation can be calculated using a quadratic formula. It is supposed that $P_{\text{out}} = P_{\text{in}}$ for the special case in which the water levels of the inlet and the outlet are set as equal in order to obtain a simpler form of the roots. Thus, the flow output rate during pumping mode can be expressed as

$$Q_{\text{out},p} = V_0 \omega \sin(\omega t) \frac{\sqrt{\xi_i}}{\sqrt{\xi_i} + \sqrt{\xi_{p,t}}}, \tag{18}$$

and the flow output rate during suction mode is

$$Q_{\text{out},s} = V_0 \omega \sin(\omega t) \frac{\sqrt{\xi_i}}{\sqrt{\xi_i} + \sqrt{\xi_{c,t}}}, \tag{19}$$

where ξ_i is the pressure loss coefficient of the inlet and $\xi_{p,t}$ and $\xi_{c,t}$ are the time-dependent pressure loss coefficients of the part enclosed by the dotted line in Figure 16.

If the time-dependent pressure loss coefficient is similar to a nozzle/diffuser element, then ξ_p is the total equivalent pressure loss coefficient over a pumping cycle and ξ_c is the total equivalent pressure loss coefficient over a suction cycle. Therefore, the quantity of the output fluid over a full cycle divided by the cycle time, which is defined as the average net flow rate, can be expressed as

$$\overline{Q_{\text{out},T}} = \frac{V_0 \omega}{\pi} \left[\frac{\sqrt{\xi_i}\left(\sqrt{\xi_c} - \sqrt{\xi_p}\right)}{\left(\sqrt{\xi_i} + \sqrt{\xi_p}\right)\left(\sqrt{\xi_i} + \sqrt{\xi_c}\right)}\right]. \tag{20}$$

According to (20), the flow output should be toward the outlet when $\sqrt{\xi_c} > \sqrt{\xi_p}$.

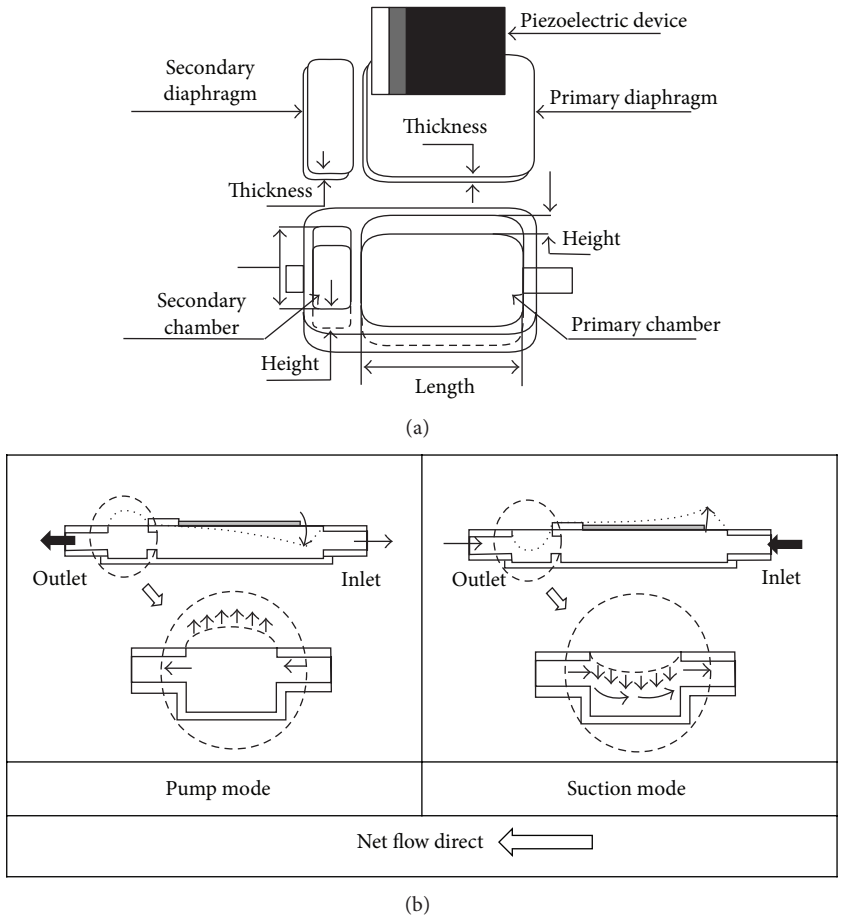

Figure 15: (a) Design of chamber; (b) operation mechanism of valveless pump.

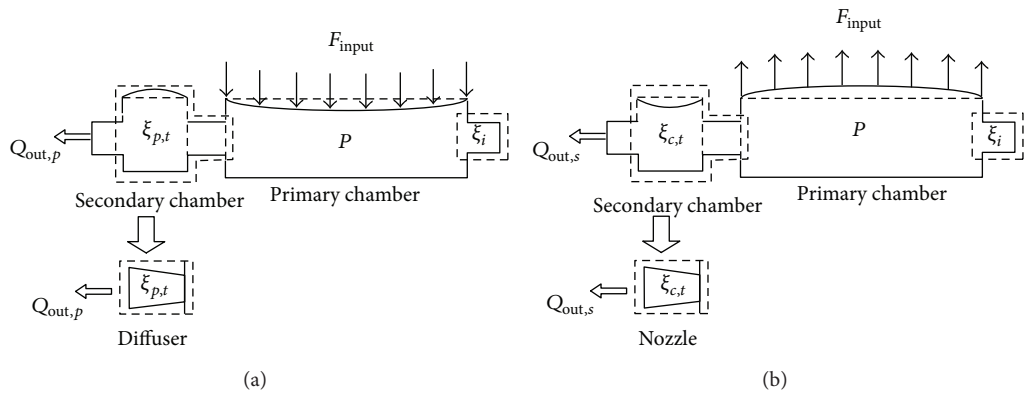

Figure 16: The similarity between the secondary chamber and a nozzle/diffuser element: (a) pump mode and (b) suction mode.

3.2. The Effect of the Secondary Chamber. Because the secondary chamber has a significant effect on the flow rate and flow direction, the dimensions of the pump have been investigated to determine optimal performance. The effect of secondary chamber is shown in Figure 17. From Figure 17, there is an evidence that the secondary chamber can be used as an element to control the flow direction. Pumps C and D show the opposite flow directions. However, pumps A and B both achieved net flow in the same flow direction through the addition of a secondary chamber. In addition, depending on the experimental results, pump A obviously has a larger flow rate than pump C. The secondary chamber not only controls

Type	Pump A	Pump B
Pump with secondary chamber		
Flow direction		
Flow rate	0.989 mL/s	0.850 mL/s
Type	Pump C	Pump D
Pump without secondary chamber		
Flow direction	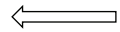	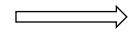
Flow rate	0.088 mL/s	0.088 mL/s

Figure 17: Experimental result for different types of pump.

the flow direction but also amplifies the flow rate. The result also is shown in Figure 18. The pump with secondary chamber can reach higher flow rate.

The influence of secondary chamber width and height are simulated, as shown in Figure 19. The designs of pump are listed in Table 2. Case 2 had a lower flow rate because of a narrow secondary diaphragm. The narrow secondary diaphragm caused the larger spring constant than Basic. Case 1 and Basic had similarity performance. The flow rate was further improved to 1.31 mL/s by decreasing the height of the secondary chamber (Case 3). It may increase the equivalent pressure loss coefficient during suction mode. Although the flow rate is affected by the size of the secondary chamber, the f_{opt} does not change.

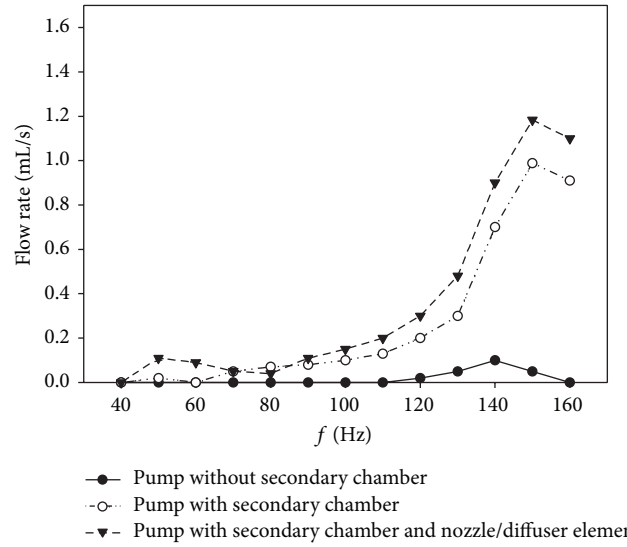

Figure 18: The comparison of flow rate with different frequency.

3.3. The Effect of Primary Chamber

3.3.1. Effect of Chamber Length and Width. The effects of chamber size are investigated in Case 4 through Case 7. From Figure 20, the optimal length of the primary chamber is 43 mm-length, and the flow rate can reach 1.128 mL/s at 180 Hz. The flow rate decreased when 41 mm-length or 45 mm-length chamber is used.

However, f_{opt} is increased to 210 Hz in Case 5 and decreased to 150 Hz in the Basic. The optimal height of the primary chamber is 4 mm. When the height of the primary chamber is reduced, the pump has a smaller hydraulic diameter, which creates a higher flow resistance. Thus, the displacement of primary diaphragm is decreased which increases the damping coefficient in (11) [25].

This result decreases the volumetric displacement and lowers the maximum flow rate from 0.989 to 0.367 mL/s when the height of the primary chamber is decreased from 4 to 1 mm. As shown in Figure 21, the flow rate and f_{opt} are both highly dependent on the height of the primary chamber: the f_{opt} decreases as the height of the primary chamber decreases.

3.3.2. Effect of Diaphragm Thickness. The performance of 0.5 mm-thick diaphragm is the optimal choice in terms of flow rate, as shown in Figure 22. According to (12), the 0.7 mm-thick diaphragm leads to a higher equivalent spring constant. Therefore, as the same actuating power, the displacement of the diaphragm and the flow rate are decreased. Though the thinner diaphragm leads to a large displacement, the 0.3 mm-thick diaphragm does not work better than the 0.5 mm-thick diaphragm because the diaphragm with the smaller K_{diaph} is squeezed by the liquid such that it expands during pumping mode. Therefore, the volume of the outflow is less than the volumetric displacement.

Table 2: The geometric dimension of pump design.

Case no.	Design of primary chamber				Design of secondary chamber			
	Length (mm)	Width (mm)	Height (mm)	Diaphragm thickness (mm)	Length (mm)	Width (mm)	Height (mm)	Diaphragm thickness (mm)
Basic	45	28	4	0.5	7	20	4	0.5
1	45	28	4	0.5	7	28	4	0.5
2	45	28	4	0.5	7	12	4	0.5
3	45	28	4	0.5	7	20	2	0.5
4	43	28	4	0.5	7	20	4	0.5
5	41	28	4	0.5	7	20	4	0.5
6	45	28	3	0.5	7	20	4	0.5
7	45	28	2	0.5	7	20	4	0.5
8	45	28	1	0.5	7	20	4	0.5
9	45	28	4	0.3	7	20	4	0.5
10	45	28	4	0.7	7	20	4	0.5

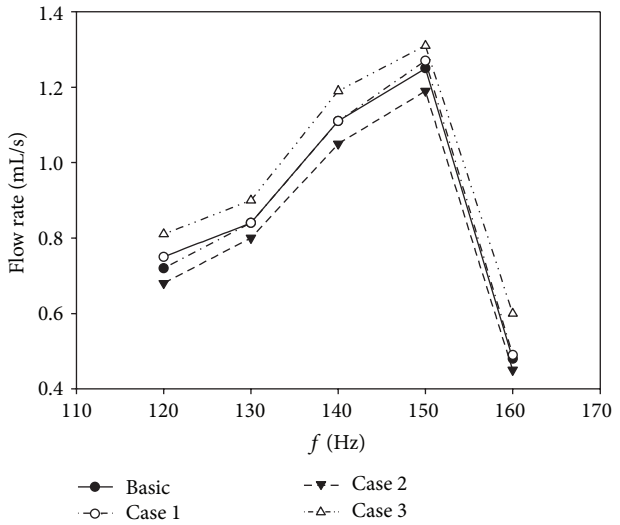

Figure 19: The simulated flow rate of different secondary pumps.

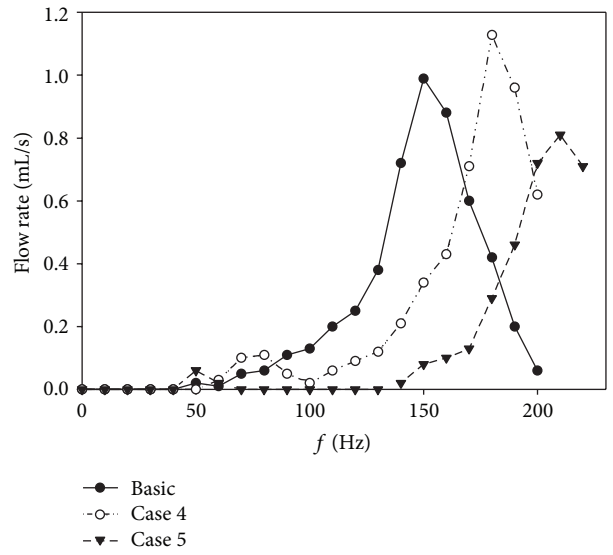

Figure 20: The measured flow rate with different primary length.

3.3.3. Effect of Nozzle/Diffuser. A nozzle/diffuser element was installed to the pump inlet, as shown in Figure 23. The optimal diffuser angle and aspect ratio has been investigated for a one-sided actuating micropump. According to previous studies [26], the preferred diffuser angle for a nozzle/diffuser element when paired with a one-sided actuating piezoelectric valveless micropump is between 9° and 12°. In this study, the nozzle/diffuser element was designed with an angle of 12° and an aspect ratio of 9.5. The experimental results indicate that the maximum flow rate of the micropump can be further improved from 0.989 mL/s to 1.183 mL/s at 150 Hz by adding a nozzle/diffuser element, as shown in Figure 18.

4. The Application of One-Sided Actuating Micropump on Fuel Cell

A novel design for proton exchange membrane fuel cells with a piezoelectric air pump (PZT-PEMFC) [27–29], which is an actuator for pumping air into the cathode chamber, offers better performance with higher current generation. In the traditional pseudo bipolar design, the cathodes are outside the cell so that the membrane electrode assembly (MEA) can reacts with air by natural convection. However, the novel pseudo bipolar design consisted of two cells, with two outside anodes and two inside cathodes that shared a common PZT vibrating device to pump airflow, as shown in Figure 24. The experimental device of PZT-PEMFC is shown in Figure 25. In this chapter, the performance of PEMFC with piezoelectric air pump is discussed below.

4.1. The Actuating Mechanism. In a PZT-PEMFC bicell, two diffuser elements are applied to induce a larger air flow rate, as shown in Figure 26. The geometrical parameters of the diffuser, including the diffuser angle (θ) and the aspect ratio (AR), affect pump performance. The lumped system was

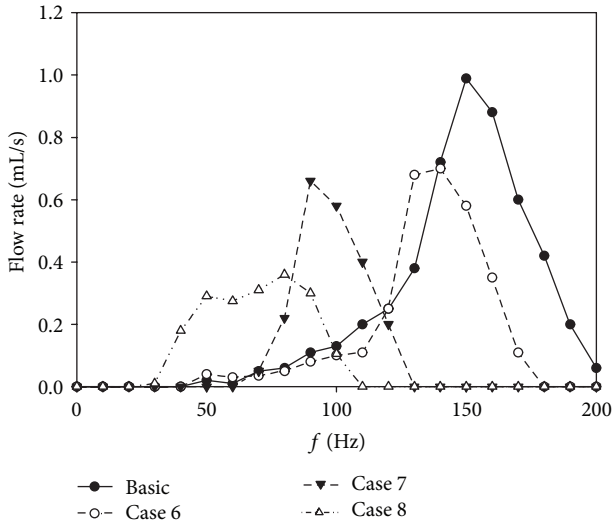

FIGURE 21: The measured flow rate with different primary height.

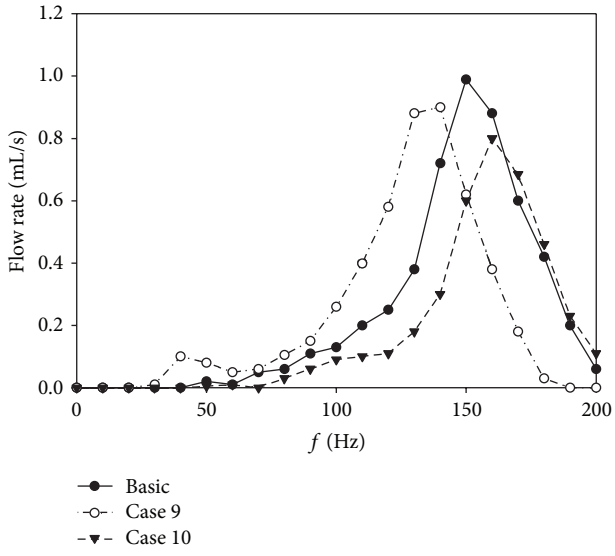

FIGURE 22: The measured flow rate with different diaphragm thickness in primary chamber.

applied to analyze the characteristics of the valveless PZT pumping system [24].

As shown in Figure 27, the time variation method was conducted for the following: exhaust mode ($P_c > P_{\text{out}} > P_{\text{in}}$), supply mode ($P_{\text{out}} > P_{\text{in}} > P_c$), and transition mode ($P_{\text{out}} > P_c > P_{\text{in}}$). An assumption was made that the inlet pressure, P_{in}, was always smaller than the outlet pressure, P_{out}, due to the nozzle/diffuser design. In the suction mode, the diaphragm moved outward and the cathode chamber volume increased, which caused the chamber pressure to be lower than the atmospheric pressure. Thus, the air was sucked into the chamber. In the pump mode, the diaphragm moved inward and the cathode chamber volume decreased. Because the pressure inside the cell was higher than the atmospheric pressure, the air was pushed into the catalyst layer and the resulting water was pumped out of the cell.

Between the pump mode and the suction mode, a transition mode occurred when the outlet pressure was higher than the chamber and inlet pressures, $P_{\text{out}} > P_c > P_{\text{in}}$. To analyze the air flow rate of the PZT-PEMFC system, the system's control volume was chosen in the cathode chamber. The equation of motion for the PZT device was a sine function given by

$$\vec{V}_{\text{pzt}} = \frac{d}{dt}\left[-\Lambda * \sin\left(2\pi f t\right)\right]. \tag{21}$$

Thus, by using the Reynolds Transport Theorem and the continuity equation, the air flow rate can be written as

$$Q_c = \frac{1}{R}\frac{\partial}{\partial t}\int_{CV}\frac{P}{T}d\text{V} + \rho\vec{V}_{\text{pzt}}A_{\text{pzt}}. \tag{22}$$

The inlet flow from the nozzle and diffuser could be found by using the diffuser element theory and the continuity equation as follows:

$$\begin{aligned} Q_{\text{in},1} &= C_n\sqrt{(P_{\text{out}} - P_c)} \quad \text{for the air inflow from left to right,} \\ Q_{\text{in},r} &= C_d\sqrt{(P_{\text{out}} - P_c)} \quad \text{for the air inflow from right to left,} \end{aligned} \tag{23}$$

where the conductivity coefficient can be separated into nozzle, C_n, and diffuser, C_d :

$$\begin{aligned} C_n &= \frac{A}{\sqrt{(1/2)\,\xi_n\rho}}, \\ C_d &= \frac{A}{\sqrt{(1/2)\,\xi_d\rho}}. \end{aligned} \tag{24}$$

Thus, the inlet flow rate is given as follows:

$$Q_{\text{in}} = Q_{\text{in},1} + Q_{\text{in},r}. \tag{25}$$

4.2. The Effect of Aspect Ratio. The aspect ratio (AR) is defined as the cathode channel path divided by the channel opening width. The performances under different aspect ratios at a smaller diffuser angle $\theta = 5^\circ$ were investigated, shown in Figure 28. The channel opening width is 1mm for different AR, so the channel length is equal to the aspect ratio.

Figure 29 shows the *I-V* curve with different AR, and it indicates that the performance of fuel cell do not improve continuously with AR increasing. For a lower aspect ratio of 5.63, the *I-V* curves dropped in the regions of concentration losses because the pressure difference between the cathode chamber and the surroundings was not strong enough to provide sufficient air. For a higher aspect ratio of 16.88, the performance didn't improve, although it can provide the larger pressure difference. The reason for this is that the blocking phenomenon occurred inside the diffuser element.

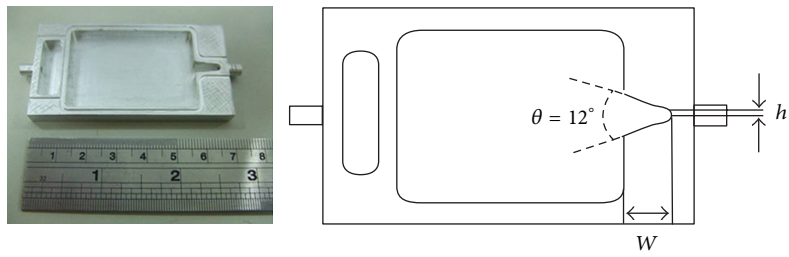

Figure 23: Schematic view of the valveless pump with nozzle/diffuser element.

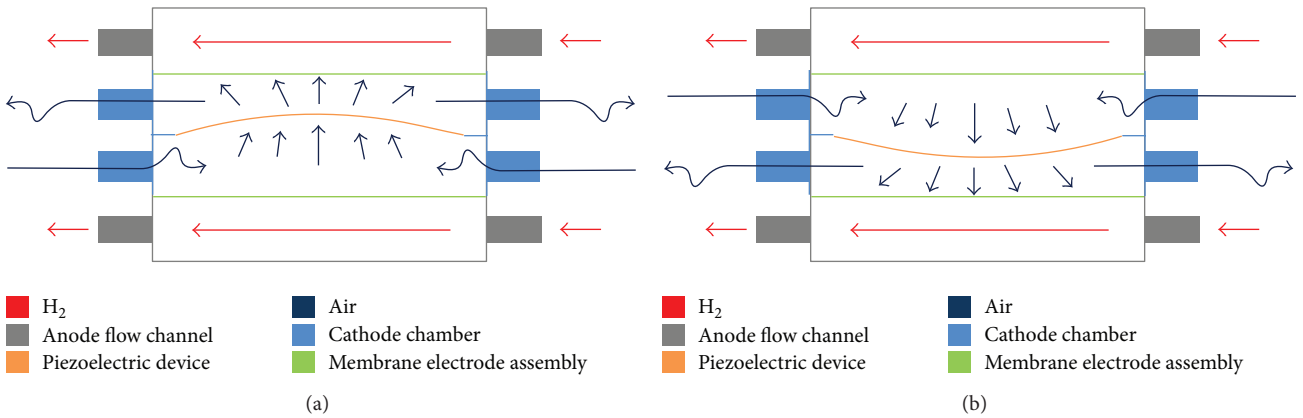

Figure 24: Operation modes of the PZT-PEMFC bicell: (a) pump mode for the upper cell and suction mode for lower cell and (b) suction mode for the upper cell and pump mode for lower cell.

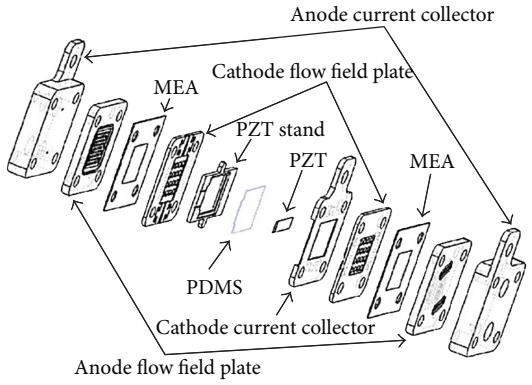

Figure 25: An exploded drawing of the PZT-PEMFC bicell.

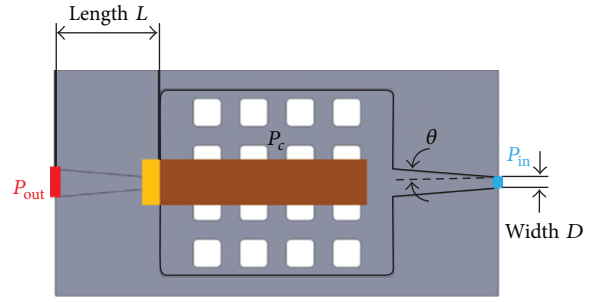

Figure 26: The cathode chamber design of the PZT-PEMFC bicell.

4.3. Influence of PZT Vibration Frequencies. While the actuating piezoelectric air pump works at the resonant frequency, the vibration amplitude of PZT can reach the maximum to intake more air into the chamber to enhance the performance of fuel cell. In this study, a diffuser $\theta = 5^\circ$ was utilized to attain higher actuation pressure. The results shows that the performance of fuel cell increases with frequency from 120 Hz to 180 Hz and causes more air sucked into. The maximum current reached 0.41 A at $f = 180$ Hz, which was almost three times greater than the case without PZT vibration ($f = 0$ Hz). The I-V curve with different frequency is shown in Figure 30.

4.4. Advantages of the One-Sided Pump in Fuel Cell. The piezoelectric actuating pump is used to compress the air into cathode chamber inside the bicell, which is different from the other designs that expose cathode to the ambient air. The active cathode with PZT device produces a forced convection in the small cathode chamber. In addition, the active cathode pumps out water vapor and solve the flooding problems in cathode. The design of piezoelectric air pump can improve the performance of fuel cell effectively.

The piezoelectric PEMFC with a nozzle and diffuser design further improved the fuel cell performance by adjusting an appropriate aspect ratio (AR) of the diffuser elements. Also, the nozzle/diffuser design can direct the air flow to

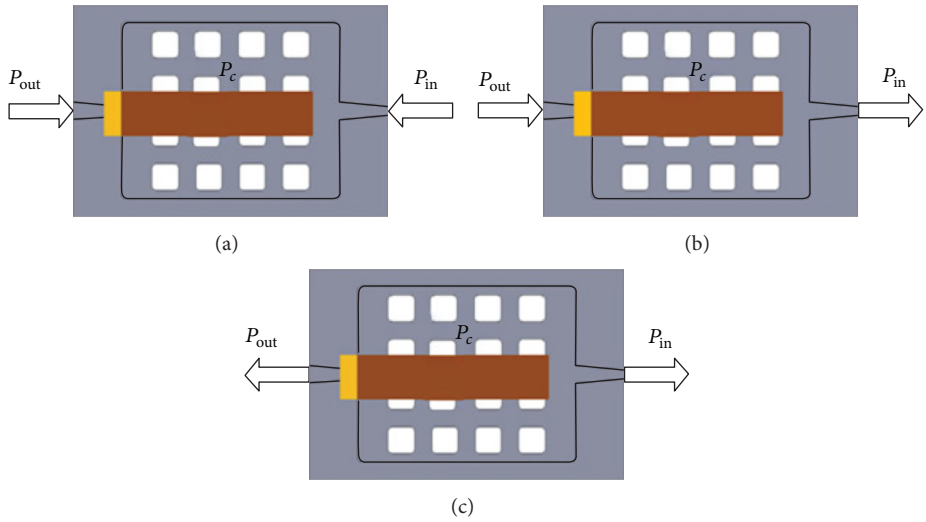

FIGURE 27: The flow modes during the actuating process (a) suction mode (b) transition mode (c) pump mode.

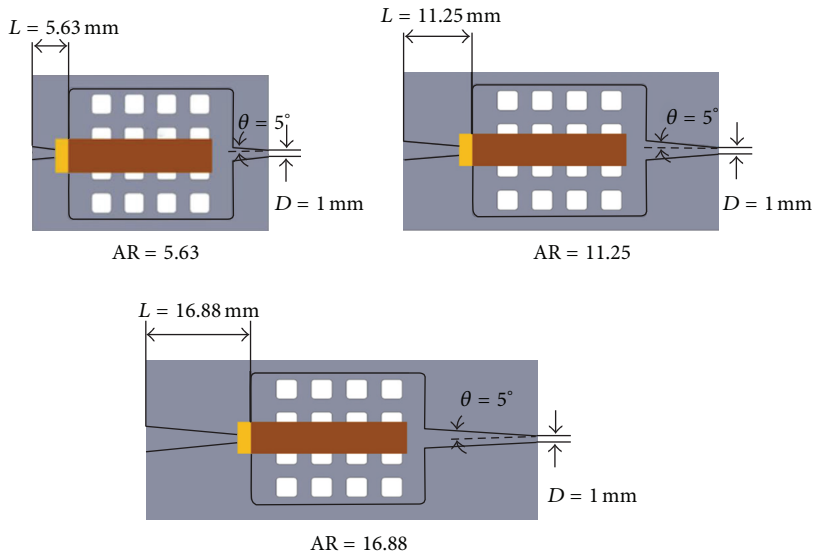

FIGURE 28: Different diffuser designs of the PZT-PEMFC.

prevent the backflow which may affect the performance of fuel cell.

5. Conclusion

Three types of one-sided actuating piezoelectric micropumps have been studied and applied in liquid or gas flow. The major conclusions from this study are summarized below.

(1) In the first type, the one-sided actuating micropump with two check valves can enhance the flow rate to prevent the back flow in suction mode and keeping flow in one direction. Moreover, the frequency modulator may be applied in the micropump to reach the maximum flow rate higher than 5.0 mL/s. However, the resonant frequencies of pump and valve may lose their harmonic motion and drop the actuating force in a higher frequency and a longer time period.

(2) In the second type, for the one-sided actuating valveless micropump with secondary chamber, the secondary chamber plays a key role in the application of the valveless micropump. It not only keeps the flow in one direction but also make the flow rate of the pump to reach 0.989 mL/s. Moreover, a nozzle/diffuser element is applied to the valveless micropump to avoid the fatigue of valve and increases its reliability, the flow rate can be further improved to 1.183 mL/s at a frequency of 150 Hz.

(3) The amplitude of the piezoelectric device can be changed and enlarged to improve the performance of micropump by using a frequency modulator. The

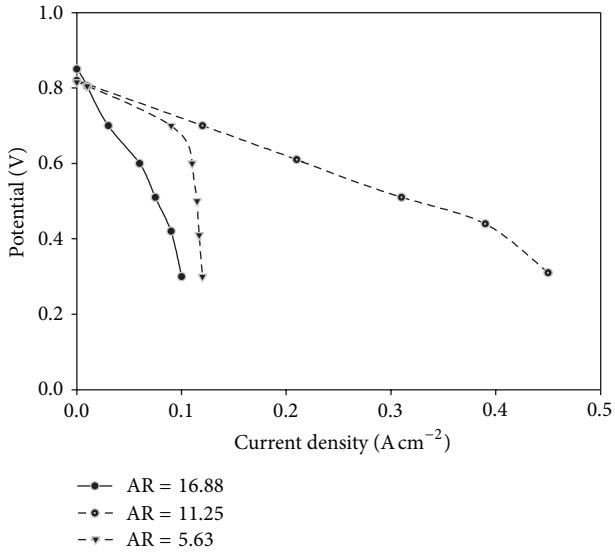

Figure 29: I-V curves under different aspect ratios in the PZT-PEMFC at $T = 40^{\circ}$C, $f = 180$ Hz, and $\theta = 5^{\circ}$.

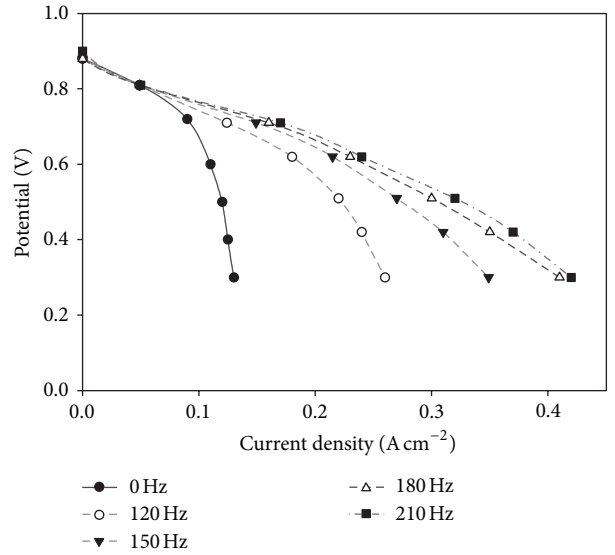

Figure 30: The I-V curves under different PZT vibration frequencies at $T = 30^{\circ}$C, AR = 11.25, and $\theta = 5^{\circ}$.

maximum flow rate can be adjusted from 14.6 mL/min to 26 mL/min at 45 Hz and ±100 V.

(4) In the third type, the piezoelectric pump is regarded as an air pump in the application of a microfuel cell system, which can pump more inlet air to increase the fuel/air reaction and further increase the performance of fuel cell. Furthermore, the design of nozzle/diffuser in outlet/inlet can prevent the backflow to make the fuel cell have a better performance.

References

[1] S. Böhm, W. Olthuis, and P. Bergveld, "A plastic micropump constructed with conventional techniques and materials," *Sensors and Actuators A*, vol. 77, no. 3, pp. 223–228, 1999.

[2] C. Yamahata, F. Lacharme, Y. Burri, and M. A. M. Gijs, "A ball valve micropump in glass fabricated by powder blasting," *Sensors and Actuators B*, vol. 110, no. 1, pp. 1–7, 2005.

[3] E. Stemme and G. Stemme, "A valveless diffuser/nozzle-based fluid pump," *Sensors and Actuators A*, vol. 39, no. 2, pp. 159–167, 1993.

[4] A. Olsson, G. Stemme, and E. Stemme, "Diffuser-element design investigation for valve-less pumps," *Sensors and Actuators A*, vol. 57, no. 2, pp. 137–143, 1996.

[5] W. L. Benard, H. Kahn, A. H. Heuer, and M. A. Huff, "Thin-film shape-memory alloy actuated micropumps," *Journal of Microelectromechanical Systems*, vol. 7, no. 2, pp. 245–251, 1998.

[6] O. Francais, I. Dufour, and E. Sarraute, "Analytical static modelling and optimization of electrostatic micropumps," *Journal of Micromechanics and Microengineering*, vol. 7, no. 3, pp. 183–185, 1997.

[7] A. Wego, H.-W. Glock, L. Pagel, and S. Richter, "Investigations on thermo-pneumatic volume actuators based on PCB technology," *Sensors and Actuators A*, vol. 93, no. 2, pp. 95–102, 2001.

[8] C. R. de Lima, S. L. Vatanabe, A. Choi, P. H. Nakasone, R. F. Pires, and E. C. Nelli Silva, "A biomimetic piezoelectric pump: computational and experimental characterization," *Sensors and Actuators A*, vol. 152, no. 1, pp. 110–118, 2009.

[9] J. Kan, K. Tang, G. Liu, G. Zhu, and C. Shao, "Development of serial-connection piezoelectric pumps," *Sensors and Actuators A*, vol. 144, no. 2, pp. 321–327, 2008.

[10] P. Skafte-Pedersen, D. Sabourin, M. Dufva, and D. Snakenborg, "Multi-channel peristaltic pump for microfluidic applications featuring monolithic PDMS inlay," *Lab on a Chip*, vol. 9, no. 20, pp. 3003–3006, 2009.

[11] M. Holtappels, M. Stubbe, and J. Gimsa, "Ac-field-induced fluid pumping in microsystems with asymmetric temperature gradients," *Physical Review E*, vol. 79, no. 2, Article ID 026309, 10 pages, 2009.

[12] E.-G. Kim, J.-G. Oh, and B. Choi, "A study on the development of a continuous peristaltic micropump using magnetic fluids," *Sensors and Actuators A*, vol. 128, no. 1, pp. 43–51, 2006.

[13] H. K. Ma, B. R. Hou, H. Y. Wu, C. Y. Lin, J. J. Gao, and M. C. Kou, "Development and application of a diaphragm micropump with piezoelectric device," *Microsystem Technologies*, vol. 14, no. 7, pp. 1001–1007, 2008.

[14] H.-K. Ma, B.-R. Hou, C.-Y. Lin, and J.-J. Gao, "The improved performance of one-side actuating diaphragm micropump for a liquid cooling system," *International Communications in Heat and Mass Transfer*, vol. 35, no. 8, pp. 957–966, 2008.

[15] H.-K. Ma, B.-R. Chen, J.-J. Gao, and C.-Y. Lin, "Development of an OAPCP-micropump liquid cooling system in a laptop," *International Communications in Heat and Mass Transfer*, vol. 36, no. 3, pp. 225–232, 2009.

[16] H. K. Ma, H. C. Su, and J. Y. Wu, "Study of an innovative one-sided actuating piezoelectric valveless micropump with a secondary chamber," *Sensors and Actuators A*, vol. 171, no. 2, pp. 297–305, 2011.

[17] J. Kan, Z. Yang, T. Peng, G. Cheng, and B. Wu, "Design and test of a high-performance piezoelectric micropump for drug delivery," *Sensors and Actuators A*, vol. 121, no. 1, pp. 156–161, 2005.

[18] J. M. Gere, *Mechanics of Materials*, Brooks Cole, Pacific Grove, Calif, USA, 5th edition, 2001.

[19] L. D. Landau and E. M. Lifshitz, *Theory of Elasticity*, Pergamon, Oxford, UK, 1986.

[20] W.-J. Sheu, R.-T. Huang, and C.-C. Wang, "Influence of bonding glues on the vibration of piezoelectric fans," *Sensors and Actuators A*, vol. 148, no. 1, pp. 115–121, 2008.

[21] L. S. Pan, T. Y. Ng, X. H. Wu, and H. P. Lee, "Analysis of valveless micropumps with inertial effects," *Journal of Micromechanics and Microengineering*, vol. 13, no. 3, pp. 390–399, 2003.

[22] L. S. Pan, T. Y. Ng, G. R. Liu, K. Y. Lam, and T. Y. Jiang, "Analytical solutions for the dynamic analysis of a valveless micropump—a fluid-membrane coupling study," *Sensors and Actuators A*, vol. 93, no. 2, pp. 173–181, 2001.

[23] V. Ziebart, O. Paul, U. Münch, J. Schwizer, and H. Baltes, "Mechanical properties of thin films from the load deflection of long clamped plates," *Journal of Microelectromechanical Systems*, vol. 7, no. 3, pp. 320–328, 1998.

[24] A. Ullmann, "The piezoelectric valve-less pump—performance enhancement analysis," *Sensors and Actuators A*, vol. 69, no. 1, pp. 97–105, 1998.

[25] S. S. Rao, *Mechanical Vibrations*, Pearson Prentice Hall, New Jersey, NJ, USA, 4th edition, 2004.

[26] Y. C. Hsiao, *Numerical analysis of a valveless One-side actuating piezoelectric micopup [M.S. thesis]*, National Taiwan University, Taipei, Taiwan, 2009.

[27] H.-K. Ma, S.-H. Huang, J.-S. Wang, C.-G. Hou, C.-C. Yu, and B.-R. Chen, "Experimental study of a novel piezoelectric proton exchange membrane fuel cell with nozzle and diffuser," *Journal of Power Sources*, vol. 195, no. 5, pp. 1393–1400, 2010.

[28] H.-K. Ma, J.-S. Wang, and Y.-T. Chang, "Development of a novel pseudo bipolar piezoelectric proton exchange membrane fuel cell with nozzle and diffuser," *Journal of Power Sources*, vol. 196, no. 8, pp. 3766–3772, 2011.

[29] H.-K. Ma, J.-S. Wang, W.-H. Su, and W.-Y. Cheng, "The performance of a novel pseudo-bipolar bi-cell piezoelectric proton exchange membrane fuel cell with a smaller nozzle and diffuser," *Journal of Power Sources*, vol. 196, no. 18, pp. 7564–7571, 2011.